# 7.5 GHz Near-Zero Temperature Coefficient of Frequency Lithium Niobate Resonator

Kangfu Liu, *Student Member, IEEE*, Yaoqing Lu, *Student Member, IEEE*, and Tao Wu, *Senior Member, IEEE*

***Abstract*— This work presents a low temperature coefficient of frequency (TCF) and high-performance S4 mode acoustic resonator based on 128°Y $LiNbO_3/SiO_2$/a-Si/Si (trap-rich layer assisted $LiNbO_3$-on-insulator, TR-LNOI) substrate. The electromechanical coupling, quality factor, and TCF are optimized for S4 mode by adjusting the thickness ratio of stack layers and the geometry design of the inter-digital transducer. The optimized resonators exhibit a TCF of resonant frequency as low as 0.24 ppm/K, an electromechanical coupling ($k^2$) of 14.8%, a maximum quality factor ($Q_{max}$) of 1406 at 7.43 GHz, resulting a $k^2 \cdot Q_{max}$ of 208. This work greatly extends the limit of $f_s \cdot k^2 \cdot Q_{max}$ for suspended thin-film resonators to 7.43 × 208 = 1545 with a near-zero TCF of resonant frequency.**

***Index Terms*— Near-zero TCF, high FoM, high performance, lithium niobate, TR-LNOI, S4 mode, acoustic resonator.**

## I. Introduction

THE increasing demand for faster data transmission and processing, mainly for 5G mobile systems, requires filters with high frequencies and large bandwidths. Piezoelectric micro-electro-mechanical system (MEMS) acoustic filters have been extensively used for radio frequency (RF) wireless systems, due to their advantages of low insertion loss, high rejection, and small footprint. 5G new radio (NR) proposed in C-band (4-8 GHz) has fractional bandwidths (FBWs) as high as 13% [1]. Without lumped element based bandwidth widening techniques [2], the FBW of filters based on resonators are fundamentally constrained by the electromechanical coupling ($k^2$) of the resonators. Such a high frequency and large FBW requirements challenge the existing surface acoustic wave (SAW) (typically $f < 3.5$ GHz) resonators, aluminum nitride (AlN) thin film bulk acoustic resonators (FBAR) ($k^2 \sim 7\%$), and the scandium-doped aluminum nitride (AlScN) resonators that struggle in the tradeoff between $k^2$ and quality factor ($Q$) [3].

Manuscript received 27 October 2022; revised 27 November 2022 and 14 December 2022; accepted 18 December 2022. Date of publication 19 December 2022; date of current version 27 January 2023. This work was supported in part by the National Natural Science Foundation of China under Grant 61874073, in part by the Lingang Laboratory under Grant LG-QS-202202-05, and in part by the Double First-Class Initiative Fund of ShanghaiTech University. The review of this letter was arranged by Editor N. Barniol. *(Corresponding author: Tao Wu.)*

Kangfu Liu and Yaoqing Lu are with the School of Information Science and Technology, ShanghaiTech University, Shanghai 201210, China, also with the Shanghai Institute of Microsystem and Information Technology, Chinese Academy of Sciences, Shanghai 200050, China, and also with the University of Chinese Academy of Sciences, Beijing 100049, China.

Tao Wu is with the School of Information Science and Technology, ShanghaiTech University, Shanghai 201210, China, also with the Shanghai Institute of Microsystem and Information Technology, Chinese Academy of Sciences, Shanghai 200050, China, also with the University of Chinese Academy of Sciences, Beijing 100049, China, and also with the Shanghai Engineering Research Center of Energy Efficient and Custom AI IC, Shanghai 201210, China (e-mail: wutao@shanghaitech.edu.cn).

Color versions of one or more figures in this letter are available at https://doi.org/10.1109/LED.2022.3230911.

Digital Object Identifier 10.1109/LED.2022.3230911

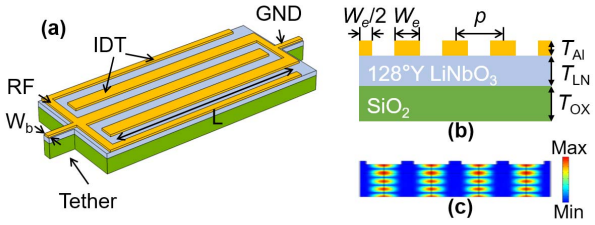


Fig. 1. (a) Mock-up view and (b) Cross-sectional view of the proposed resonator, and geometry dimensions are labeled in detail. (c) Displacement distribution of S4 mode.

The first-order asymmetric lamb wave (A1 mode) excited by the inter-digital transducer (IDT) based on Z- and 128°Y-cut $LiNbO_3$ demonstrated a $k^2$ as large as 30-46% is a promising solution [4], [5], [6] to meet the FBW requirement of 5G NR. However, the worse temperature coefficients of frequency (TCF) of the uncompensated A1 [7], FBAR [8], [9] of $LiNbO_3$ resonators are typically in the range of -70∼-100 ppm/K, which is far from the requirement of transitions gaps [10] in an 85°C temperature range. Further more, when the frequency reaches 5 GHz, the thickness of $LiNbO_3$ is approximately around 300 nm [9], [11], leading to a fragile suspended structure, challenges of spurious mode suppression [12] and strong TCF contribution from electrodes [8], [9]. The attempts so far to improve the TCF may bring spurious mode as well as degradation of $Q$ in both A3 mode [7] and S4 mode [13] resonators.

In this work, we designed and fabricated a C-band low TCF $LiNbO_3$ S4 mode resonators based on 128°Y $LiNbO_3/SiO_2$/amorphous-Si (a-Si) layers. Thanks to the optimization of design and the low RF-loss of trap-rich layer assisted $LiNbO_3$-on-insulator (TR-LNOI) substrate, the fabricated resonators achieve a $Q_{max}$ of 1406, $k^2$ of 14.8% at 7.43 GHz, and a near-zero TCF of resonant frequency with a nearly spurious-free response.

## II. Design and Fabrication

Fig. 1 includes the mock-up view, cross-sectional schematic as well as the mode shape of the S4 mode resonator. 128°YX-cut is selected to effectively excite the thickness-

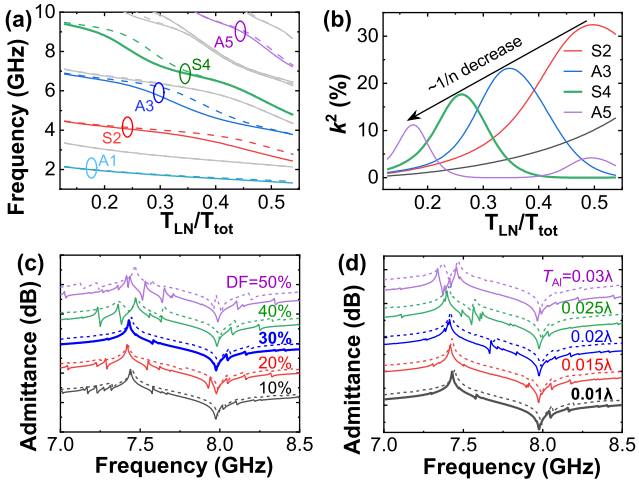


Fig. 2. (a) Simulated dispersion curve for a bi-layer of $LiNbO_3$ on top of 685 nm $SiO_2$. The solid/dashed lines represent the frequencies under electrically open/short boundaries. (b) Electromechanical coupling versus thickness ratio $T_{LN}/T_{tot}$. Simulated admittance under different (c) duty factor and (d) electrode thickness, when $T_{LN}/T_{tot}$ is 1/4 and $\lambda$=10 μm. The solid/dashed lines represent mechanical free/damping boundaries. The curves are shifted to clearly show the difference.

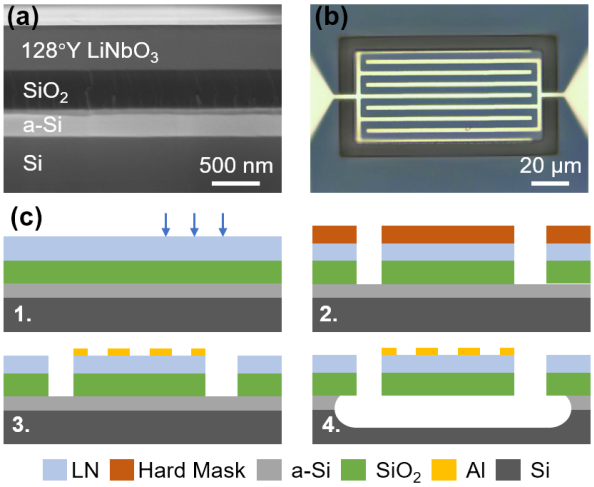


Fig. 3. (a) SEM photo of the cross-section of the start wafer. (b) Optical image for a fabricated resonator. (c) Fabrication process: 1. Thinned the start wafer with the Ar+ ion beam; 2. A hard mask ($SiO_2$) is deposited, and release holes are etched by inductively coupled plasma-enhanced reactive ion etching (ICP-RIE); 3. Remove the hard mask and lift off 100 nm Al; 4. Vapor $XeF_2$ release.

shear (TS) lamb waves (A1, S2, A3…), which is close to 120°YX-cut that has maximum $k_{15}^2$ [14]. The $SiO_2$ layer serves as a supporting layer as well as the temperature compensation layer for tuning TCF. The a-Si layer serves as the trap-rich layer avoiding parasitic surface conductive effect [15] between the $SiO_2$ layer and the semiconductor support substrate, which helps to improve the RF-loss and $Q$ of resonators. The weighted electrode design is adopted for higher $Q$ inspired by [16] and [17].

To maximize the $k^2$ of the resonator, Berlincourt's formula [18] is used to estimate the $k^2$.

$$k^2 \approx \frac{8}{\pi^2} k_s^2 s_n \tag{1}$$

where $k_s^2$ is the static coupling coefficient; $s_n$ is a scaling factor defined as the $k^2$ ratio of $n^{th}$ order TS mode to $1^{st}$ mode. The electric field and stress distribution in [18] are adopted in the estimation. In a single piezoelectric plate, $s_n = 1/n^2$ (when $n$ is odd). Instead, in the stack layers include a piezoelectric plate and a non-piezoelectric plate with similar material properties, when the thickness of $LiNbO_3$ layer ($T_{LN}$) is $1/n$ of the total thickness ($T_{tot}$), a maximum value of $s_n$ can be obtained:

$$s_{n,max} \approx 1/n \tag{2}$$

The characteristics of TS mode and admittance curves are captured by COMSOL® *Multiphysics*. Fig. 2 (a) shows the dispersion curve for TS mode dependence of the thickness ratio of $T_{LN}/T_{tot}$, while wavelength $\lambda = 10\,\mu m$. The $k^2$ is calculated by [6]:

$$k^2 = \frac{\pi^2}{8} \frac{f_{open}^2 - f_{short}^2}{f_{short}^2} \tag{3}$$

where $f_{short}$ and $f_{open}$ are frequencies under electrically short and open boundaries, respectively. As shown in Fig. 2 (b), the maximum $k^2$ is inversely proportional to $n$, at $T_{LN}/T_{tot} \approx 1/n$. S4 mode demonstrates high frequency (~7.5 GHz) and moderate $k^2$ (~17%).

To suppress the spurious modes, the duty factor (DF) and electrode thickness ($T_{Al}$) should be carefully selected. Figs. 2 (c)-(d) show the simulated admittance response with different DF, $T_{Al}$ and mechanical boundaries. Most spurious modes in the propagation direction can be eliminated by applying the damping boundaries but lead to a lower $Q$. DF = 0.3 is selected for consideration of fabrication limit, and $T_{Al} = 0.01\lambda$ (100 nm) is selected for spurious suppression.

The scanning electron microscopy (SEM) photo for the cross-section of the start wafer is shown in Fig. 3 (a), including 685 nm $LiNbO_3$/685 nm $SiO_2$/300 nm a-Si layers. The optical image in Fig. 3 (b) shows the electrode weighted design is well implemented. Resonators with a small anchor beam width $W_b$ and a beam length $L_b$ of ~ $\lambda$ tend to possess higher $Q$ [19], thus $W_b$ and $L_b$ are designed to 3 and 10 μm, respectively. Fig. 3 (c) shows the fabrication steps. By ion beam milling, $T_{LN}$ is thinned to 270 nm, leading the thickness ratio $T_{LN}/T_{tot}$ approximately to 0.28.

## III. Result and Discussion

The measurements were performed by using a Keysight® vector network analyzer (PNA-L-N5234B) equipped with 200 μm ground-signal-ground probes. Modified Butterworth-Van Dyke (mBVD) equivalent circuit was used for fitting, while the $k^2$, Bode-$Q$, and FoM = $k^2 \times Q_{max}$ were calculated as in previous works [20], where $Q_{max}$ is the maximum value of Bode-$Q$. The admittance of devices was extracted by de-embedding the open structure on the same chip [21].

Fig. 4 (a) shows the dependence of simulated and measured resonant frequency $f_s$ of S4 mode resonators on $\lambda$. $f_s$ only change 1.3%, even though $\lambda$ varies from 6 to 16 μm, which indicates that the resonant frequency of S4 mode is nearly exclusively determined by the thickness and weakly correlated with $\lambda$. Noticeably, the $TCF_s$ for $f_s$ of an S4 mode resonator can be tuned by $\lambda$ like the SAW devices [22], which is verified by the simulation and measurement data shown in Fig. 4 (b). Temperature coefficients and material properties for

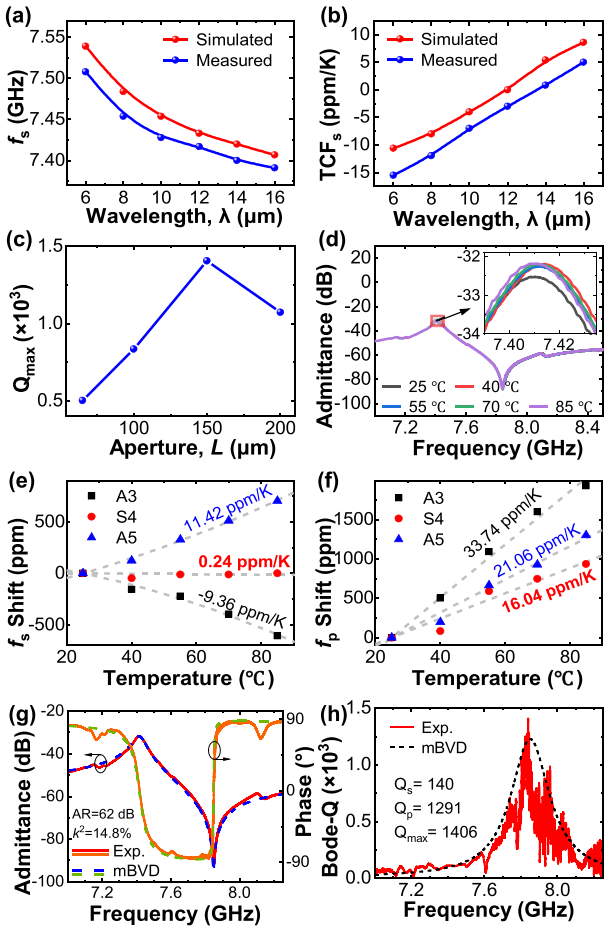


Fig. 4. The dependency of simulated and measured (a) resonant frequency ($f_s$) and (b) TCF$_s$ for $f_s$ on wavelength λ. (c) $Q_{max}$ varies with aperture $L$. (d) Admittance and frequency shift of (e) $f_s$ and (f) $f_p$ under different temperatures of a resonator with λ of 14 μm and $L$ of 150 μm. Measured and mBVD fitted (g) admittance, phase, and (h) Bode-$Q$ of a resonator with optimized structure.

different materials used in the simulation can be found in [23]. A near-zero TCF$_s$ can be obtained when $\lambda$ is about 14 μm. The balance between anchor loss and electrode loss can be achieved by adjusting the aperture [24], Fig. 4 (c) shows that a maximum $Q_{max}$ is obtained at $L = 150$ μm. With the above optimization, a resonator with high $Q$ value and low TCF can be realized simultaneously. The admittance of an optimized S4 mode resonator under different temperatures shown in Fig. 4 (d) demonstrates almost temperature-independent performance without any degradation.

Figs. 4 (e)–(f) shows the frequency shifts of resonant frequency $f_s$ and anti-resonant frequency $f_p$ that vary with temperatures in different modes and the quadratic fits used to calculate TCFs. The TCFs are labeled on the corresponding curves. There are significant differences in TCFs between different modes, which is also reported by [7], but the related mechanism still needs to be further studied. For the S4 mode, the TCF of $f_s$ (TCF$_s$) is 0.24 ppm/K, while the TCF of $f_p$ (TCF$_p$) is 16.04 ppm/K. Figs. 4 (g)-(h) show the measured and mBVD fitted admittance, phase and Bode-$Q$ curves. It is gratifying that a compensated S4 mode resonator demonstrates an admittance ratio (AR) of 62 dB, $k^2$ of 14.8%, $Q_{max}$ of 1406, resulting in an FoM of 208.

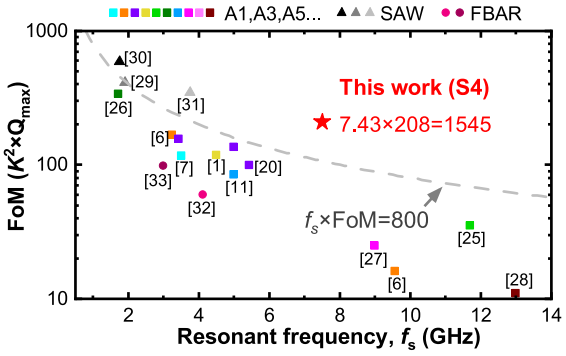


Fig. 5. A comparison of the reported resonator with prior reported resonators in terms of FoM and $f_s$. Note that the highest quality factor is adopted for this comparison, in which $Q_{max}$ [20], [29], [30], [31], [32]; $Q_s$ [6], [7], [11]; $Q_p$ [33]; $Q_m$ [25], [26], [27], [28].

Fig. 5 illustrates a plot of FoM as a function of $f_s$, which evaluates the performance of the reported resonators and compare with state-of-arts [6], [7], [11], [20], [25], [26], [27], [28], [29], [30], [31], [32], [33]. Note that the reported highest quality factor among $Q_{max}$, $Q_s$, $Q_p$ and $Q_m$ is adopted for this comparison, where $Q_s$, $Q_p$ and $Q_m$ represent the quality factor of $f_s$, $f_p$ and the motion branch in mBVD model, respectively. Considering high FoM tends to possess low insertion loss, while $f_s$ and $Q_{max}$ are mutually compromised, $f_s \times$FoM is selected as the comprehensive performance metric. Except for the recently developed SAW devices on heterogeneous substrates [30], [31], other resonators fall in the region with $f_s \times \text{FoM} \leq 800$.

This work demonstrates the highest $f_s \times$FoM so far and shows a significant breakthrough among the resonator with suspended structure (including TS mode resonator and FBAR), which greatly pushes the $f_s \times$FoM limit from 800 to 1545 (7.43 GHz×208) as well as a near-zero TCF$_s$. The reasons for high comprehensive performance and low TCF are: (a) The choice of suitable LN cut and optimal thickness ratio to excite the S4 mode with high $k^2$, (b) The suitable design of anchor and IDT aperture to achieve a balance between electric loss and anchor loss, (c) The introduction of an a-Si layer to reduce the RF-loss from the substrate, (d) The utilization of the tuning effect of wavelength ($\lambda$) to TCF.

## IV. Conclusion

In this work, we successfully demonstrated a 7.5 GHz and high-performance S4 mode resonator on 128°Y-cut TR-LNOI substrate with near-zero TCF of resonant frequency. With optimization of geometry dimensions, a fabricated resonator achieved a $Q_{max}$ of 1406, $k^2$ of 14.8% at 7.43 GHz and a TCF$_s$ of 0.24 ppm/K with a nearly spurious-free response. This work paves the way for preeminent filtering in communications above 6 GHz and opens up more possibilities for resonators with high comprehensive performance co-existing with low TCF.

## Acknowledgment

The authors would like to thank Soft Matter Nanofab (No. SMN180827) and ShanghaiTech Quantum Device Laboratory (SQDL) for the device fabrication support.

## REFERENCES


[1] Y. Yang, R. Lu, L. Gao, and S. Gong, "4.5 GHz lithium niobate MEMS filters with 10% fractional bandwidth for 5G front-ends," *J. Microelectromech. Syst.*, vol. 28, no. 4, pp. 575–577, Aug. 2019, doi: 10.1109/jmems.2019.2922935.

[2] A. Gao, K. Liu, J. Liang, and T. Wu, "AlN MEMS filters with extremely high bandwidth widening capability," *Microsyst. Nanoeng.*, vol. 6, no. 1, pp. 1–11, Sep. 2020, doi: 10.1038/s41378-020-00183-5.

[3] C. Moe, R. H. Olsson, P. Patel, Z. Tang, M. D'Agati, M. Winters, R. Vetury, and J. Shealy, "Highly doped AlScN 3.5 GHz XBAW resonators with 16% k2eff for 5G RF filter applications," in *Proc. IEEE Int. Ultrason. Symp. (IUS)*, Sep. 2020, pp. 1–4, doi: 10.1109/IUS46767.2020.9251412.

[4] M. Kadota, T. Ogami, K. Yamamoto, H. Tochishita, and Y. Negoro, "High-frequency Lamb wave device composed of MEMS structure using $LiNbO_3$ thin film and air gap," *IEEE Trans. Ultrason., Ferroelectr., Freq. Control*, vol. 57, no. 11, pp. 2564–2571, Nov. 2010, doi: 10.1109/TUFFC.2010.1722.

[5] V. Plessky, S. Yandrapalli, P. J. Turner, L. G. Villanueva, J. Koskela, and R. B. Hammond, "5 GHz laterally-excited bulk-wave resonators (XBARs) based on thin platelets of lithium niobate," *Electron. Lett.*, vol. 55, no. 2, pp. 98–100, Nov. 2018, doi: 10.1049/el.2018.7297.

[6] R. Lu, Y. Yang, S. Link, and S. Gong, "A1 resonators in 128° Y-cut lithium niobate with electromechanical coupling of 46.4%," *J. Microelectromech. Syst.*, vol. 29, pp. 313–319, Jun. 2020, doi: 10.1109/jmems.2020.2982775.

[7] A. E. Hassanien, R. Lu, and S. Gong, "Near-zero drift and high electromechanical coupling acoustic resonators at >3.5 GHz," *IEEE Trans. Microw. Theory Techn.*, vol. 69, no. 8, pp. 3706–3714, Aug. 2021, doi: 10.1109/TMTT.2021.3079497.

[8] M. Bousquet, G. Enyedi, J. Dechamp, M. Zussy, P. S. P. Kuisseu, F. Mazen, C. Billard, A. Reinhardt, M. Bertucchi, P. Perreau, G. Castellan, C. Maeder-Pachurka, D. Mercier, J. Delprato, A. Borzi, and S. Sejil, "Single-mode high frequency $LiNbO_3$ film bulk acoustic resonator," in *Proc. IEEE Int. Ultrason. Symp. (IUS)*, Oct. 2019, pp. 84–87, doi: 10.1109/ULTSYM.2019.8925617.

[9] M. Bousquet, P. Perreau, C. Maeder-Pachurka, A. Joulie, F. Delaguillaumie, J. Delprato, G. Enyedi, G. Castellan, C. Eleouet, T. Farjot, C. Billard, and A. Reinhardt, "Lithium niobate film bulk acoustic wave resonator for sub-6 GHz filters," in *Proc. IEEE Int. Ultrason. Symp. (IUS)*, Sep. 2020, pp. 1–4, doi: 10.1109/IUS46767.2020.9251654.

[10] *IEEE Standard for Local and Metropolitan Area Networks—Part 16: Air Interface for Fixed Broadband Wireless Access Systems*, IEEE Standard 802.16-2004 (Revision of IEEE Standard 802.16-2001), 2004, pp. 1–915.

[11] S. Yandrapalli, S. E. K. Eroglu, V. Plessky, H. B. Atakan, and L. G. Villanueva, "Study of thin film $LiNbO_3$ laterally excited bulk acoustic resonators," *J. Microelectromech. Syst.*, vol. 31, no. 2, pp. 217–225, Apr. 2022, doi: 10.1109/JMEMS.2022.3143354.

[12] S. Gong, R. Lu, Y. Yang, L. Gao, and A. E. Hassanien, "Microwave acoustic devices: Recent advances and outlook," *IEEE J. Microw.*, vol. 1, no. 2, pp. 601–609, Apr. 2021, doi: 10.1109/JMW.2021.3064825.

[13] A. E. Hassanien and S. Gong, "An acoustic resonator with electromechanical coupling of 16% and low TCF at 5.4 GHz," in *Proc. IEEE Int. Ultrason. Symp. (IUS)*, Sep. 2021, pp. 1–4, doi: 10.1109/IUS52206.2021.9593546.

[14] R. Lu and S. Gong, "RF acoustic microsystems based on suspended lithium niobate thin films: Advances and outlook," *J. Micromech. Microeng.*, vol. 31, no. 11, Nov. 2021, Art. no. 114001, doi: 10.1088/1361-6439/ac288f.

[15] B. Rong, J. N. Burghartz, L. K. Nanver, B. Rejaei, and M. van der Zwan, "Surface-passivated high-resistivity silicon substrates for RFICs," *IEEE Electron Device Lett.*, vol. 25, no. 4, pp. 176–178, Apr. 2004, doi: 10.1109/LED.2004.826295.

[16] A. Gao and J. Zou, "Extremely high *Q* AlN Lamb wave resonators implemented by weighted electrodes," in *IEDM Tech. Dig.*, Dec. 2019, pp. 34.5.1–34.5.4, doi: 10.1109/IEDM19573.2019.8993608.

[17] S. Gong and G. Piazza, "Figure-of-merit enhancement for laterally vibrating lithium niobate MEMS resonators," *IEEE Trans. Electron Devices*, vol. 60, no. 11, pp. 3888–3894, Nov. 2013, doi: 10.1109/TED.2013.2281734.

[18] S.-H. Chang, N. N. Rogacheva, and C. C. Chou, "Analysis of methods for determining electromechanical coupling coefficients of piezoelectric elements," *IEEE Trans. Ultrason., Ferroelectr., Freq. Control*, vol. 42, no. 4, pp. 630–640, Jul. 1995, doi: 10.1109/58.393106.

[19] Y.-Y. Chen, Y.-T. Lai, and C.-M. Lin, "Finite element analysis of anchor loss in AlN Lamb wave resonators," in *Proc. IEEE Int. Freq. Control Symp. (FCS)*, May 2014, pp. 1–5, doi: 10.1109/FCS.2014.6859875.

[20] T. Kimura, M. Omura, Y. Kishimoto, and K. Hashimoto, "Comparative study of acoustic wave devices using thin piezoelectric plates in the 3–5-GHz range," *IEEE Trans. Microw. Theory Techn.*, vol. 67, no. 3, pp. 915–921, Mar. 2019, doi: 10.1109/TMTT.2018.2890661.

[21] M. Koolen, J. Geelen, and M. Versleijen, "An improved de-embedding technique for on-wafer high-frequency characterization," in *Proc. Bipolar Circuits Technol. Meeting*, Sep. 1991, pp. 188–191, doi: 10.1109/BIPOL.1991.160985.

[22] J. Shen, S. Fu, R. Su, Z. Lu, H. Xu, P. Liu, R. Wang, T. Chen, X. He, F. Zeng, C. Song, W. Wang, and F. Pan, "A low-loss wideband SAW filter with low drift using multilayered structure," *IEEE Electron Device Lett.*, vol. 43, no. 8, pp. 1371–1374, Aug. 2022, doi: 10.1109/LED.2022.3185003.

[23] M.-H. Li, C.-Y. Chen, R. Lu, Y. Yang, T. Wu, and S. Gong, "Temperature stability analysis of thin-film lithium niobate $SH_0$ plate wave resonators," *J. Microelectromech. Syst.*, vol. 28, no. 5, pp. 799–809, Oct. 2019, doi: 10.1109/JMEMS.2019.2934126.

[24] L. Colombo, A. Kochhar, G. Vidal-Álvarez, and G. Piazza, "High-figure-of-merit X-cut lithium niobate MEMS resonators operating around 50 MHz for large passive voltage amplification in radio frequency applications," *IEEE Trans. Ultrason., Ferroelectr., Freq. Control*, vol. 67, no. 7, pp. 1392–1402, Jul. 2020, doi: 10.1109/TUFFC.2020.2972293.

[25] S. Link, R. Lu, Y. Yang, A. E. Hassanien, and S. Gong, "An A1 mode resonator at 12 GHz using 160 nm lithium niobate suspended thin film," in *Proc. IEEE Int. Ultrason. Symp. (IUS)*, Sep. 2021, pp. 1–4, doi: 10.1109/IUS52206.2021.9593341.

[26] Y. Yang, R. Lu, T. Manzaneque, and S. Gong, "1.7 GHz Y-cut lithium niobate MEMS resonators with FoM of 336 and fQ of $9.15\times10^{12}$," in *IEEE MTT-S Int. Microw. Symp. Dig.*, Jun. 2018, pp. 563–566, doi: 10.1109/MWSYM.2018.8439516.

[27] Y. Zhang, L. Wang, Y. Zou, Q. Xu, J. Liu, Q. Wang, A. Tovstopyat, W. Liu, C. Sun, and H. Yu, "Lithium niobate thin film based A3 mode resonators with high effective coupling coefficient of 6.72%," in *Proc. IEEE 34th Int. Conf. Micro Electro Mech. Syst. (MEMS)*, Jan. 2021, pp. 466–469, doi: 10.1109/MEMS51782.2021.9375462.

[28] Y. Yang, R. Lu, L. Gao, and S. Gong, "10–60-GHz electromechanical resonators using thin-film lithium niobate," *IEEE Trans. Microw. Theory Techn.*, vol. 68, no. 12, pp. 5211–5220, Dec. 2020, doi: 10.1109/TMTT.2020.3027694.

[29] T. Takai, H. Iwamoto, Y. Takamine, H. Yamazaki, T. Fuyutsume, H. Kyoya, T. Nakao, H. Kando, M. Hiramoto, T. Toi, M. Koshino, and N. Nakajima, "High-performance SAW resonator on new multilayered substrate using $LiTaO_3$ crystal," *IEEE Trans. Ultrason., Ferroelectr., Freq. Control*, vol. 64, no. 9, pp. 1382–1389, Sep. 2017, doi: 10.1109/TUFFC.2017.2738119.

[30] J. Wu, S. Zhang, Y. Chen, P. Zheng, L. Zhang, H. Yao, Z. Li, X. Zhao, K. Huang, T. Wu, and X. Ou, "Advanced surface acoustic wave resonators on $LiTaO_3/SiO_2$/sapphire substrate," *IEEE Electron Device Lett.*, vol. 43, no. 10, pp. 1748–1751, Oct. 2022, doi: 10.1109/LED.2022.3200418.

[31] R. Su, S. Fu, Z. Lu, J. Shen, H. Xu, Z. Xu, R. Wang, C. Song, F. Zeng, W. Wang, and F. Pan, "Over GHz bandwidth SAW filter based on 32° Y-X $LN/SiO_2$/poly-Si/Si heterostructure with multilayer electrode modulation," *Appl. Phys. Lett.*, vol. 120, no. 25, Jun. 2022, Art. no. 253501, doi: 10.1063/5.0092767.

[32] M. Bousquet, P. Perreau, A. Joulie, F. Delaguillaumie, C. Maeder-Pachurka, G. Castellan, G. Envedi, J. Delprato, F. Mazen, A. Reinhardt, I. Huyet, T. Laroche, A. Clairet, and S. Ballandras, "4.2 GHz $LiNbO_3$ film bulk acoustic resonator," in *Proc. IEEE Int. Ultrason. Symp. (IUS)*, Sep. 2021, pp. 1–4, doi: 10.1109/IUS52206.2021.9593774.

[33] M. Gorisse, R. Bauder, H.-J. Timme, H.-P. Friedrich, L. Dours, P. Perreau, A. Ravix, R. Lefebvre, G. Castellan, C. Maeder-Pachurka, M. Bousquet, and A. Reinhardt, "High frequency $LiNbO_3$ bulk wave resonator," in *Proc. Joint Conf. IEEE Int. Freq. Control Symp. Eur. Freq. Time Forum (EFTF/IFC)*, Apr. 2019, pp. 1–2, doi: 10.1109/FCS.2019.8856017.